# Determination of cross sections and oscillator strengths for argon by electron-energy-loss spectroscopy

G. P. Li, T. Takayanagi, K. Wakiya, and H. Suzuki
*Department of Physics, Sophia University, Chiyoda-ku, Tokyo 102, Japan*

T. Ajiro, S. Yagi, S. S. Kano, and H. Takuma
*Institute for Laser Science, University of Electro-Communications, Chofu-shi, Tokyo 182, Japan*
(Received 13 October 1987)

Absolute differential cross sections for the $3p^6\,{}^1S_0 \rightarrow 3p^5(^2P_{1/2})4s,(^2P_{3/2})4s$ excitation in argon have been measured at impact energies of 400 and 500 eV, and at scattering angles between 1.75° and 10.3° by electron-energy-loss spectroscopy. The integrated cross sections and generalized oscillator strengths (GOS's) have also been determined at 400 and 500 eV. The optical oscillator strengths have been determined, by extrapolating the GOS's to zero momentum transfer, as $0.222^{+0.02}_{-0.03}$ for the $(^2P_{1/2})4s$ state and $0.058^{+0.005}_{-0.008}$ for the $(^2P_{3/2})4s$ state. These data are compared with the results of other optical measurements in the vacuum-ultraviolet region. The errors are estimated to be less than 14%.

## I. INTRODUCTION

Because of the high content of argon in the mixture of gases used in rare-gas–halogen excimer lasers, for example, about 90% Ar in KrF lasers, the investigation of the excitation cross sections for argon by electron impact is very important to analyze quantitatively the energy convertibility of the lasers. Besides this, we need precise excitation cross sections and oscillator strengths for resonance lines in argon to use them as secondary standards of absolute cross sections, by which measurements of relative cross sections for inner-shell and subshell ionizations can be made absolute.[1]

There is a shortage of theoretical calculations for the excitations in argon, because argon is a heavier atom, so that the *LS* coupling is not applicable to it. As for experimental studies, for transitions from the ground state $(3s^23p^6\,{}^1S_0)$ to $3p^5(^2P_{1/2})4s$ and $3p^5(^2P_{3/2})4s$ states in argon, which correspond to 1048- and 1067-Å resonance lines, respectively, a few results have been reported, and most of them have been obtained by optical spectroscopy. De Jongh and van Eck[2] determined the excitation cross section for the $(^2P_{1/2})4s$ state by measuring the self-absorption of radiation as a function of gas pressure. McConkey and Donaldson[3] and Mentall and Morgan[4] determined excitation cross sections for both states by observing vacuum-ultraviolet radiation due to the deexcitations, which include some cascade contributions from upper excited states. On the other hand, Chutjian and Cartwright[5] determined the differential and integrated cross sections at electron-impact energies between 16 and 100 eV by electron-energy-loss spectroscopy (EELS), which does not have any cascade contributions.

However, there exist serious discrepancies among the results; for example, the excitation cross section for the $(^2P_{3/2})4s$ state of Ref. 3 is nearly three times larger than that of Ref. 5. Existing literature also shows that up to now the optical oscillator strengths (OOS's) for the 1048- and 1067-Å lines have almost been measured with optical methods.

In the present work, differential cross sections (DCS's) and generalized oscillator strengths (GOS's) for the $(^2P_{1/2})4s$ and $(^2P_{3/2})4s$ states in argon are carefully determined by EELS. The OOS's are also determined by EELS, in which many difficulties in the optical-absorption technique are avoided, and therefore more accurate results can be expected.

## II. APPARATUS AND EXPERIMENTAL PROCEDURES

The apparatus used is composed of an electron gun, an energy selector, an interaction region, an energy analyzer, and four sets of electrostatic lenses, as schematically shown in Fig. 1. Both the selector and the analyzer are of

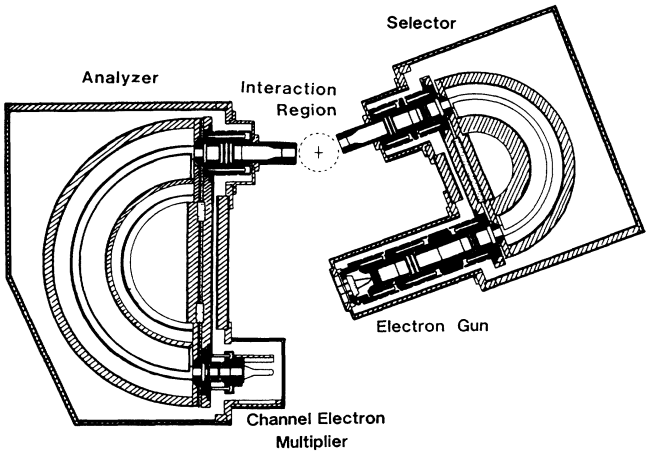


FIG. 1. Schematic diagram of the experimental apparatus. The target beam in the interaction region is perpendicular to the paper surface.

 

a simulated hemispherical electrostatic type.[6] The mean trajectory radius is 50 mm for the selector and 80 mm for the analyzer. The energy resolution is 25–40 meV full width at half maximum (FWHM) at 30-nA electron current and 10–500-eV impact energy. The energy selector is rotatable around the collision center from $-5°$ to 110°. All of these parts are enclosed in a vacuum chamber, as shown in Fig. 2. The main chamber is evacuated by a 10-in. diffusion pump (DP), while the energy selector and energy analyzer with their lens systems are differentially pumped by two 4-in. diffusion pumps to minimize the corrosion of some active target gases. Perfluoropolyether (called Fomblin, made by Montedison Co.) is used for the pump oil, because this oil is stable against chemically active gases. The ultimate vacuum of the system is $3\times10^{-7}$ Torr.

Cylinders of the electron lenses, the energy selector, and the analyzer are made of nonmagnetic stainless steel. External magnetic fields are diminished by a Permalloy metal shield, while the remaining longitudinal components of the magnetic fields are canceled by a square Helmholtz coil. Consequently, the residual magnetic fields in the interaction region are maintained to less than a few mG.

An electron beam emitted from a hairpin-type tungsten filament enters into the energy selector through the first lens. Then the monochromatized beam is accelerated by the second lens and emerges into the interaction region.

Two modes of collision schemes are utilized using this apparatus. One is the crossed-beam mode and the other is the static-target mode. In the crossed-beam mode, a target atomic beam is effused from a nozzle of 0.5-mm diameter and collides with the electron beam at right angles. In the static mode, after the main chamber is filled with a target gas, the main valve for the main chamber is closed. The target gas is pumped only through the small apertures of the selector and analyzer, so that we can treat the target gas in the interaction region like a "rest target gas."

The potential difference between the inner and outer electrodes is fixed at the appropriate value, so that the scattered electrons of a fixed energy can pass through the analyzer. After passing through the analyzer, the electrons are accelerated by the fourth lens and detected by a channel-electron multiplier. The signal originating from these scattered electrons is amplified and fed into a multichannel analyzer and then displayed as an energy-loss spectrum by means of a conventional multiscaler mode technique, in which the channel-advancing signals are made to correspond with the retarding voltage for the scattered electrons through the third lens. In the measurements of the inelastic DCS for argon, we utilized the crossed-beam mode, while in the measurements of the elastic DCS for argon and helium, which were made to examine the performance of the apparatus, we utilized the static target mode.

It is known that angular accuracy has great influence on observed signal intensities, particularly in the case of forward scattering. A calibration for scattering angles has been performed by use of the symmetry of the scattering intensity ratio $I_{2\,^1S}/I_{2\,^1P}$, corresponding to the $2\,^1S$ and the $2\,^1P$ excitations from the ground state in helium, which is known to be a steep function of scattering angle. Figure 3 shows that the true scattering angle is 0.35° less than the geometric angle of the instrument. The angular resolution of the apparatus has been determined according to the angular distribution of the direct electron beam from the energy selector, with an impact energy of 500 eV. As shown in Fig. 4, the resolution is about 0.8° (FWHM), which we consider precise enough for the present measurement.

In general, for a fixed impact energy $E_0$, the apparent DCS $d\sigma/d\Omega$ can be determined from the relation

$$\frac{d\sigma}{d\Omega}=\frac{CI}{ip}\eta(\theta)\ , \tag{1}$$

where $I$ stands for the observed signal intensity, $i$ for the electron-beam current, and $p$ for the target-gas pressure. A function $\eta(\theta)$ is the angular-dependent factor to

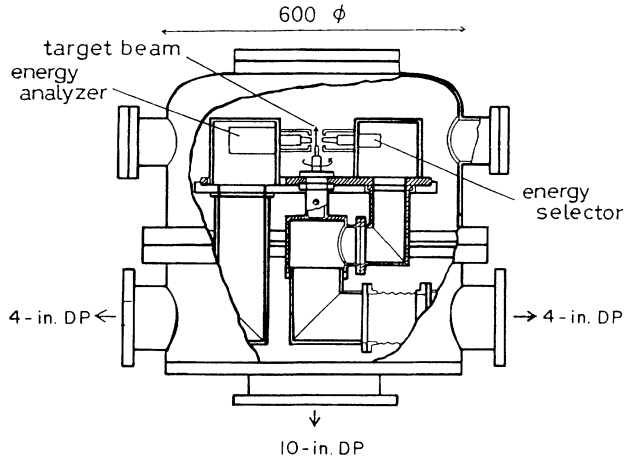


FIG. 2. Schematic diagram of the vacuum system. Diameter of the main chamber is 600 mm.

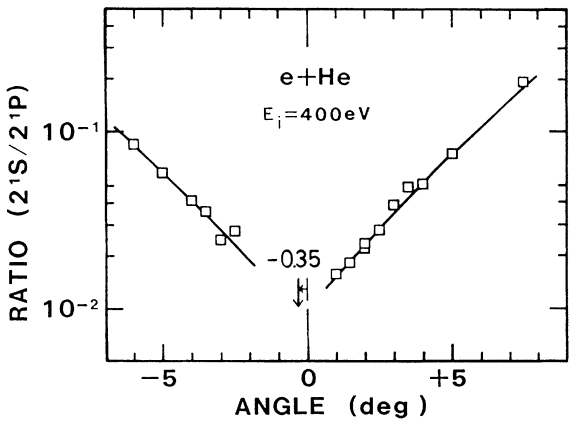


FIG. 3. Calibration for the scattering angles. The horizontal axis represents the geometric angle of the instrument. The symmetry of the inelastic scattering intensity ratio $I_{2\,^1S}/I_{2\,^1P}$ in helium shows that the zero of the scattering angle is 0.35° less than that of the geometric angle.

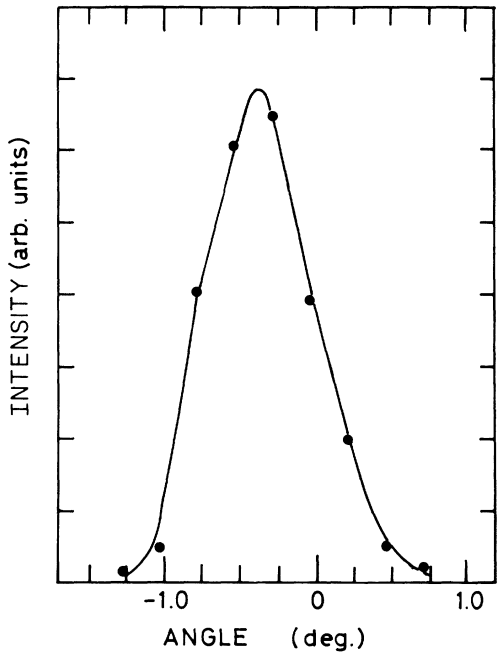


FIG. 4. Angular resolution of the apparatus, determined by the angular distribution of the direct electron beam from the energy selector.

present the effective collision volume, and it is considered to be $\sin\theta$ when scattering angle $\theta$ is larger than 3° in the static target mode. $C$ is an instrumental efficiency independent of $\theta$. Because it is difficult to determine $\eta(\theta)$ and $C$ in the crossed-beam mode, relative measurements are more frequently performed. We can cancel $\eta(\theta)$ and $C$ by observing the intensity ratio of the peaks of interest to the peak for elastic scattering. From Eq. (1), we obtain

$$\left[\frac{d\sigma}{d\Omega}\right]_{\text{inel}} \Big/ \left[\frac{d\sigma}{d\Omega}\right]_{\text{el}} = I_{\text{inel}}/I_{\text{el}} , \tag{2}$$

where the subscripts denote inelastic and elastic scattering, respectively; the experimental intensity ratio $I_{\text{inel}}/I_{\text{el}}$ is obtained as the ratio of the respective peak areas in the energy-loss spectra. According to Eq. (2), the $(d\sigma/d\Omega)_{\text{inel}}$ can be simply determined by multiplying the ratio with an absolute value of the known $(d\sigma/d\Omega)_{\text{el}}$ at the same impact energy. In this work, the absolute DCS for the elastic scattering measured by Bromberg[7] and by Jansen *et al.*[8] were plotted on the same graph. Then a fitting function was made by use of these data. We used the values calculated from this fitting function as the normalization standards.

## III. RELATIONS OF CROSS SECTIONS WITH OSCILLATOR STRENGTH

If the incidence electron energy is high enough to ensure the validity of the Born approximation, the relation connecting the DCS and GOS can be represented as[9] (in a.u.)

$$\frac{d\sigma}{d\Omega} = \frac{2}{WK^2}\left[\frac{k_f}{k_i}\right] F(K) , \tag{3}$$

where $W$ stands for the excitation energy and $F(K)$ for the GOS. The incident and scattered momenta $k_i$ and $k_f$ and the momentum transfer $K$ are defined, respectively, as

$$k_i=(2E_0)^{1/2},\quad k_f=(2E)^{1/2},\quad \mathbf{K}=\mathbf{k}_i-\mathbf{k}_f . \tag{4}$$

Now we rewrite Eq. (3) in useful form,

$$F(K)=\frac{W}{2}\frac{k_i}{k_f}K^2\left[\frac{d\sigma}{d\Omega}\right] , \tag{5}$$

from which, substituting the corresponding parameters in Eq. (5), the GOS $F(K)$ can be experimentally determined. It should be noted that if the Born approximation is valid, the GOS $F(K)$ depends only on the momentum transfer. Klump and Lassettre[10] have derived an expansion

$$F(K)=\frac{f_0}{(1+x)^6}\left[1+\sum_{n=1}^{\infty} f_n\left[\frac{x}{1+x}\right]n\right] , \tag{6}$$

where $f_0$ is the OOS, $f_n$ are coefficients, and parameter $x$ equals $(K/Y)^2$, where $Y$ is related to the ionization potential $P_i$ and excitation energy $W$ by $Y=(P_i)^{1/2}+(P_i-W)^{1/2}$. Lassettre has also demonstrated that $F(K)$ and $f_0$ are always related by

$$\lim_{K\to 0} F(K)=f_0 , \tag{7}$$

regardless of whether the validity of the Born approximation is ensured or not. This theorem suggests that one can determine the OOS $f_0$ by extrapolating the GOS to the limit $K=0$.

Furthermore, by employing both Eqs. (5) and (6), we obtain the integrated cross section

$$\sigma=2\pi\int\frac{d\sigma}{d\Omega}\sin\theta\, d\theta=\frac{2\pi}{Wk_i^2}\int F(K)d(\ln K^2) . \tag{8}$$

## IV. RESULTS AND DISCUSSION

A typical energy-loss spectrum for the excitation of argon is shown in Fig. 5, which is taken at impact energy of 400 eV and at a scattering angle of 2.3°. Our measurements show that the spectrum at an impact energy of 500 eV is almost the same as that of 400 eV. There are several peaks in the spectrum; the most intensive peak at 11.83 eV corresponds to the $(^2P_{1/2})4s$ excitation, while the adjacent peak at 11.62 eV corresponds to the $(^2P_{3/2})4s$ excitation.

The angular dependence of the intensity ratio of the $(^2P_{1/2})4s$ and $(^2P_{3/2})4s$ peaks to the elastic scattering peak is given in Fig. 6. Our absolute DCS for inelastic scattering of the $(^2P_{1/2})4s$ and $(^2P_{3/2})4s$ states in argon are shown in Fig. 7. The numerical results are given in Table I.

Using Eq. (5), we obtained the GOS for the two excitation processes. Then, by fitting these discrete data to smooth curves with the method of least squares, we obtained two approximate representations: $F_{1/2}(K)$ for the $(^2P_{1/2})4s$ state and $F_{3/2}(K)$ for the $(^2P_{3/2})4s$ state,

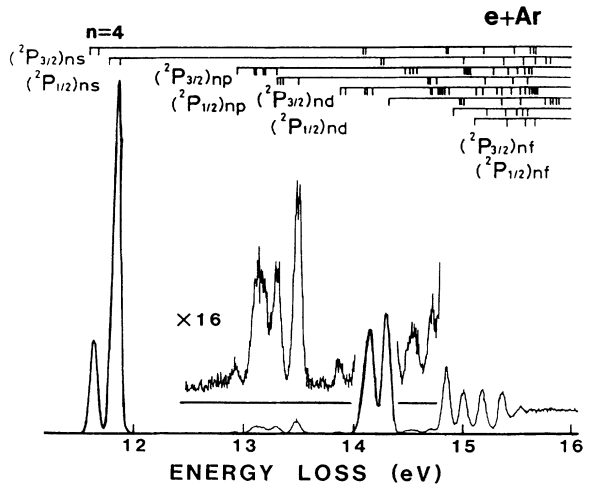


FIG. 5. Typical energy loss spectrum for the excitation of argon, taken at 400 eV and at 2.3°. The peak at 11.83 eV corresponds to the $(^2P_{1/2})4s$ state and that at 11.62 eV corresponds to the $(^2P_{3/2})4s$ state.

$$F_{1/2}(K)=\{0.222-1.026[x/(1+x)] +2.094[x/(1+x)]^2+\cdots\}/(1+x)^6 ,$$
$$F_{3/2}(K)=\{0.058-0.312[x/(1+x)] +0.743[x/(1+x)]^2+\cdots\}/(1+x)^6 . \quad (9)$$

Figure 8 shows the curves of $F_{1/2}(K)$ and $F_{3/2}(K)$ as

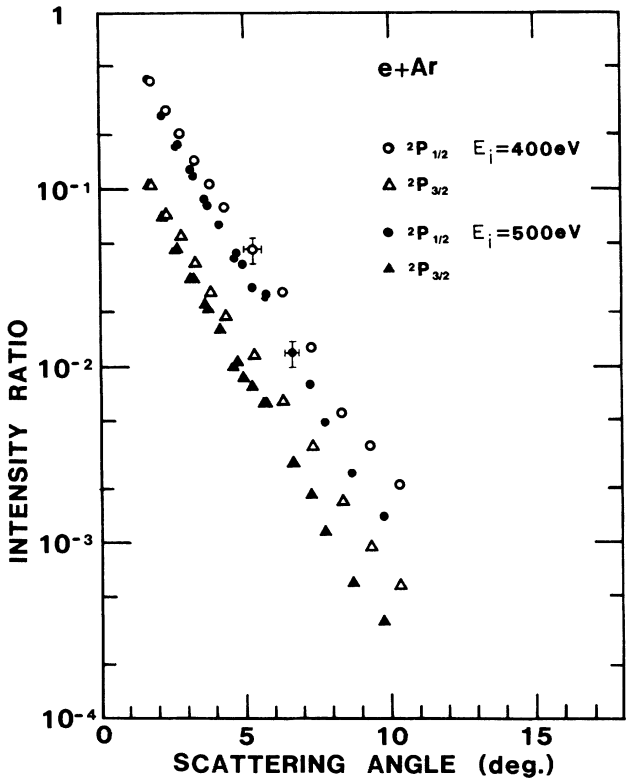


FIG. 6. Angular dependence of the intensity ratio of the $(^2P_{1/2})4s$ and $(^2P_{3/2})4s$ peaks to the elastic scattering peak.

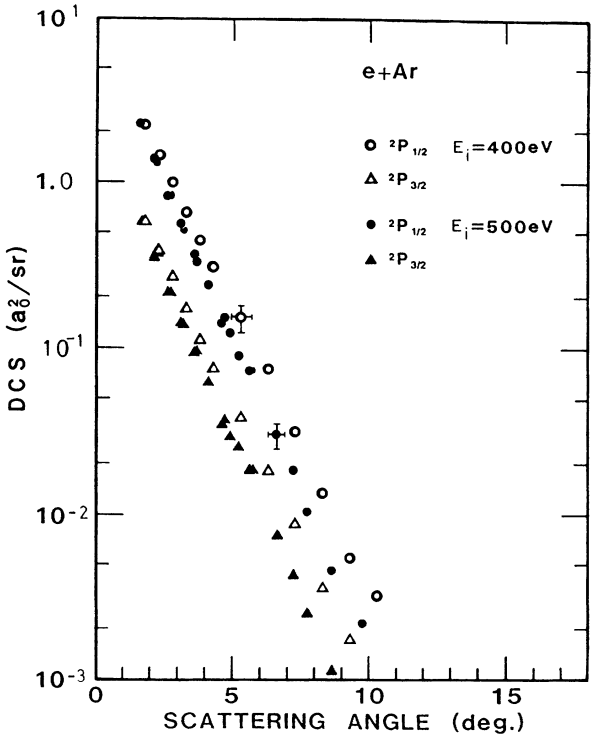


FIG. 7. Absolute differential cross sections for the excitation of the $(^2P_{1/2})4s$ and $(^2P_{3/2})4s$ states.

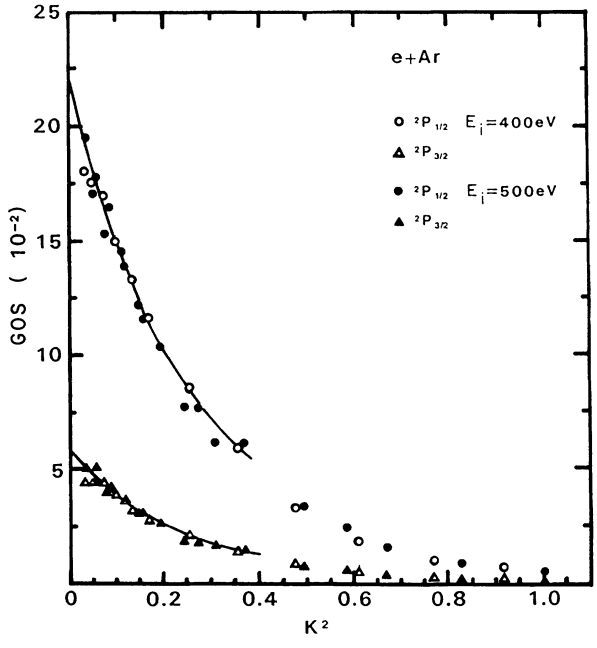


FIG. 8. Generalized oscillator strengths for the $(^2P_{1/2})4s$ and $(^2P_{3/2})4s$ states as a function of the squared momentum transfer $K^2$. Two curves have been obtained by fitting our experimental data to the Klump and Lassettre's expansion. The intercepts of the curves with the ordinate present the corresponding optical oscillator strengths.

functions of $K^2$, which have been deduced from the DCS measured at scattering angles from 1.75° to 6.65° and impact energies of 400 and 500 eV. It was found from the figure that the GOS curves for 500 eV is almost the same as that for 400 eV. The intercepts on the longitudinal axis are just the OOS, the values are $0.222^{+0.02}_{-0.03}$ for 1048 Å [$(^2P_{1/2})4s$] and $0.058^{+0.005}_{-0.008}$ for 1067 Å [$(^2P_{3/2})4s$] resonance lines. A comparison of the present results with those of other groups is given in Table II: Chamberlain *et al.*[11] determined the OOS by EELS, Lawrence[12] by observing the vacuum ultraviolet radiation by electron impact, Stacey and Vaughan[13] by observing collision broadenings, Lewis[14] by observing the pressure broadening and shifts, de Jongh and van Eck[2] by observing the self-absorption of the radiation, and Dow and Knox[15] carried out the theoretical calculation based solely on wave functions (footnote h, Table II) and based on experimental energies and the dipole matrix computed from wave functions (footnote i, Table II).

Integrated excitation cross sections at 400- and 500-eV impact energies were determined by using Eq. (8). Because the DCS rapidly decreases at larger scattering angles, as shown in Fig. 7, only at small scattering angles does the DCS make a dominant contribution to the magnitudes of the integrals. As a quantitative estimation, for the $(^2P_{3/2})4s$ excitation at 500-eV impact energy, the magnitude of the integral over the momentum transfer $K$ from 0 to 0.2 is $9.04\times10^{-2}$, from 0.2 to 0.6 is $8.63\times10^{-3}$, and from 0.6 to 1.5 is $4.04\times10^{-4}$, so that the remaining part of the integral is less than $\frac{1}{100}$ of the total over the region of $K$ larger than 1.5. For this reason, we cut the integral off at the point $K=1.5$. Once the GOS is

TABLE I. Numeral results of the intensity ratios to the elastic scattering and the absolute differential cross sections (in a.u.) for excitation of the $(^2P_{1/2})4s$ and $(^2P_{3/2})4s$ states at impact energy $E_0$. Square brackets denote the power of 10. The $(d\sigma/d\Omega)_{el}$ are determined by the interpolation and extrapolation of the results by Bromberg and Jansen *et al.*

| Angle | | Intensity ratio | | $\left[\frac{d\sigma}{d\Omega}\right]_{inel}$ | |
|---|---|---|---|---|---|
| (deg.) | $\left[\frac{d\sigma}{d\Omega}\right]_{el}$ | $P_{1/2}$ | $P_{3/2}$ | $P_{1/2}$ | $P_{3/2}$ |
| | | $E_0=400$ meV | | | |
| 1.8 | 5.57 | 4.10 [−1] | 1.07 [−1] | 2.28 | 5.95 [−1] |
| 2.3 | 5.17 | 2.85 [−1] | 7.49 [−2] | 1.48 | 3.87 [−1] |
| 2.8 | 4.81 | 2.09 [−1] | 5.65 [−2] | 1.01 | 2.72 [−1] |
| 3.3 | 4.47 | 1.47 [−1] | 3.92 [−2] | 6.58 [−1] | 1.75 [−1] |
| 3.8 | 4.15 | 1.08 [−1] | 2.69 [−2] | 4.48 [−1] | 1.12 [−1] |
| 4.3 | 3.85 | 8.04 [−2] | 1.98 [−2] | 3.09 [−1] | 7.63 [−2] |
| 5.3 | 3.32 | 4.62 [−2] | 1.19 [−2] | 1.53 [−1] | 3.95 [−2] |
| 6.3 | 2.85 | 2.65 [−2] | 6.59 [−3] | 7.56 [−2] | 1.88 [−2] |
| 7.3 | 2.45 | 1.30 [−2] | 3.60 [−3] | 3.18 [−2] | 8.82 [−3] |
| 8.3 | 2.10 | 6.52 [−3] | 1.77 [−3] | 1.37 [−2] | 3.72 [−3] |
| 9.3 | 1.80 | 3.59 [−3] | 9.67 [−4] | 6.47 [−3] | 1.74 [−3] |
| 10.3 | 1.54 | 2.18 [−3] | 6.01 [−4] | 3.36 [−3] | 9.28 [−4] |
| | | $E_0=500$ eV | | | |
| 1.75 | 5.43 | 4.21 [−1] | 1.09 [−1] | 2.29 | 5.93 [−1] |
| 2.15 | 5.13 | 2.70 [−1] | 7.04 [−2] | 1.39 | 3.61 [−1] |
| 2.25 | 5.05 | 2.63 [−1] | 7.57 [−2] | 1.35 | 3.82 [−1] |
| 2.65 | 4.76 | 1.77 [−1] | 4.66 [−2] | 8.42 [−1] | 2.22 [−1] |
| 2.75 | 4.69 | 1.80 [−1] | 4.72 [−2] | 8.46 [−1] | 2.22 [−1] |
| 3.15 | 4.43 | 1.30 [−1] | 2.24 [−2] | 5.74 [−1] | 1.44 [−1] |
| 3.25 | 4.36 | 1.19 [−1] | 3.25 [−2] | 5.21 [−1] | 1.42 [−1] |
| 3.65 | 4.11 | 8.89 [−2] | 2.30 [−2] | 3.65 [−1] | 9.47 [−2] |
| 3.75 | 4.05 | 8.14 [−2] | 2.17 [−2] | 3.30 [−1] | 8.79 [−2] |
| 4.15 | 3.81 | 6.37 [−2] | 1.66 [−2] | 2.43 [−1] | 6.31 [−2] |
| 4.65 | 3.53 | 4.12 [−2] | 1.02 [−2] | 1.46 [−1] | 3.60 [−2] |
| 4.75 | 3.48 | 4.42 [−2] | 1.09 [−2] | 1.54 [−1] | 3.80 [−2] |
| 4.95 | 3.38 | 3.77 [−2] | 8.88 [−3] | 1.27 [−1] | 3.00 [−2] |
| 5.25 | 3.22 | 2.82 [−2] | 8.06 [−3] | 9.10 [−2] | 2.60 [−2] |
| 5.75 | 2.99 | 2.55 [−2] | 6.42 [−3] | 7.62 [−2] | 1.92 [−2] |
| 6.65 | 2.60 | 1.21 [−2] | 2.92 [−3] | 3.15 [−2] | 7.58 [−3] |
| 7.25 | 2.36 | 8.08 [−3] | 1.91 [−3] | 1.91 [−2] | 4.51 [−3] |
| 7.75 | 2.18 | 4.95 [−3] | 1.18 [−3] | 1.08 [−2] | 2.57 [−3] |
| 8.65 | 1.89 | 2.51 [−3] | 6.15 [−4] | 4.74 [−3] | 1.16 [−3] |
| 9.75 | 1.58 | 1.42 [−3] | 3.73 [−4] | 2.25 [−3] | 5.90 [−4] |

experimentally determined at high impact energies, we can also calculate the integrated cross sections at lower impact energies in the frame of the Born approximation. As a result, excitation functions from the thresholds to 500 eV for the $(^2P_{1/2})4s$ and $(^2P_{3/2})4s$ states were derived. The present results are shown in Fig. 9, where

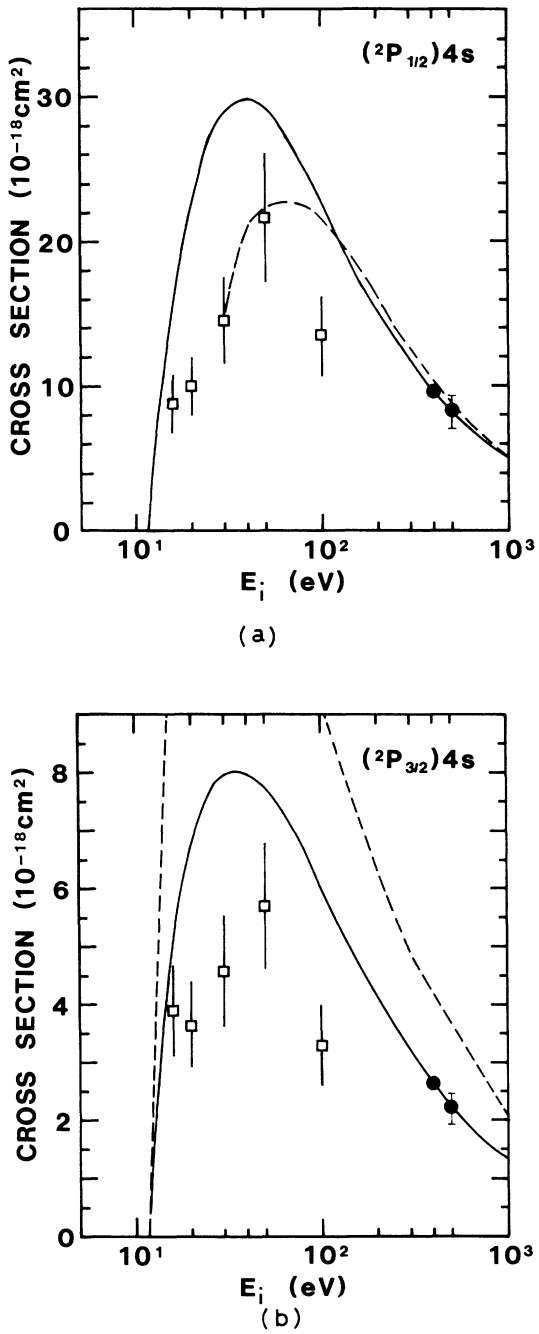


FIG. 9. Integrated excitation cross sections (a) for the $(^2P_{1/2})4s$ and (b) for the $(^2P_{3/2})4s$ state. The closed circles are our experimental results and the solid curves are derived according to the Born approximation. The dashed curves are the experimental results by McConkey *et al.* and the squares by Chutjian and Cartwright.

several data of other groups are also drawn for comparison. For the $(^2P_{1/2})4s$ excitation, the result of McConkey and Donaldson is in very good agreement with ours, while for the $(^2P_{3/2})4s$ excitation their result is about 30% larger than the present work. This discrepancy is considered to be caused by their incorrect 1048 Å to 1067 Å line intensity ratio of 2.52, which is much smaller than other existing reports, in spite of their reasonable choice of the OOS 0.22 for the $(^2P_{1/2})4s$ excitation that is very close to our data. Also, it is demonstrated in the figure that the Born approximation gives close results to the experiment at the higher-energy region, while it gives cross sections too large compared with experiments at lower energies, a well-known property of the Born approximation. The result of Chutjian and Cartwright seems to be smaller than both of McConkey *et al.* and the present work.

Errors in this measurement are mainly due to the uncertainty of the scattering angles. The causes of the errors, such as the angular resolution, deviations from the zero scattering angle, and reproducibility of the scattering angles are taken into account. Summing up these errors and taking the effect of the finite angular resolution into account (how this effect has influence on the observed results is evaluated in Appendix), the total errors are estimated to be $+9\%$ and $-14\%$, including the error due to neglecting the integral region larger than $K > 1.5$ mentioned in the preceding.

The present work may be used to improve the situation in reliability in the standard data of excitation cross sections and of the OOS determined by various methods.

## APPENDIX

In the present results, we got the angular dependence of DCS for both the $(^2P_{1/2})4s$ and $(^2P_{3/2})4s$ excitations, which can be approximated by exponential functions (Fig. 7). If we put the angular response function $f(x)$ of the apparatus as a Gaussian function, we can estimate how $d\sigma/d\Omega$ is affected by the angular resolution rather easily. Suppose $f(x)$ depends on scattering angle $x$ as

$$f(x)=\frac{1}{a\sqrt{\pi}}\exp\left[-\left[\frac{x-x_0}{a}\right]^2\right],$$

where $a$ is a parameter which shows the angular resolution of the apparatus, and the apparatus is set at $x=x_0$. The function $f(x)$ is normalized as

$$\int_{-\infty}^{\infty} f(x)dx = 1 .$$

If the $d\sigma/d\Omega$ depends on $x$ as

$$\frac{d\sigma}{d\Omega}=B\exp(-|x|/b) \quad (b>0) ,$$

the measured DCS's are represented by an averaged value

TABLE II. Comparison of the present optical oscillator strengths for $(^2P_{1/2})4s$ and $(^2P_{3/2})4s$ excitation with other results. Here, Opt. represents the optical experiments, EELS the electron energy loss spectroscopy, and Theory the theoretical calculation.

| Author | $^1S_0 \rightarrow (^2P_{1/2})4s$ | $^1S_0 \rightarrow (^2P_{3/2})4s$ |
|---|---|---|
| EELS | | |
| The present work | $0.222^{+0.02}_{-0.03}$ | $0.058^{+0.005}_{-0.008}$ |
| Chamberlain *et al.*[a] | 0.181 | 0.049 |
| Opt. | | |
| Lawrence[b] | 0.228±0.021 | 0.059±0.003 |
| Stacey and Vaughan[c] | 0.275±0.02 | 0.036±0.004 |
| Lewis[d] | 0.278±0.002 | |
| de Jongh and van Eck[e] | 0.22±0.02 | |
| McConkey and Donaldson[f] | | 0.096±0.02 |
| Theory | | |
| Dow and Knox[g] | 0.17[h] | 0.052[h] |
| | 0.20[i] | 0.049[i] |

[a]Reference 11.
[b]Reference 12.
[c]Reference 13.
[d]Reference 14.
[e]Reference 2.
[f]Reference 3.
[g]Reference 15.
[h]Based solely on wave functions.
[i]Based on experimental energies and the dipole matrix computed from wave functions.

$$\left\langle \frac{d\sigma}{d\Omega} \right\rangle = \int_{-\infty}^{\infty} f(x) \frac{d\sigma}{d\Omega} dx$$

$$= \frac{B}{a\sqrt{\pi}} \int_{-\infty}^{\infty} \exp\left[ -\left[ \frac{x - x_0}{a} \right]^2 \right] \times \exp(-|x|/b) dx$$

$$= B \exp(-x_0/b) \exp\left[ \frac{a^2}{4b^2} \right] g(x_0) ,$$

where

$$g(x_0) = \frac{1}{a\sqrt{\pi}} \int_0^{\infty} \exp\left[ -\frac{\left[ x - x_0 + \frac{a^2}{2b} \right]^2}{a^2} \right] dx$$

$$+ \frac{1}{a\sqrt{\pi}} \exp(2x_0/b) \times \int_{-\infty}^{0} \exp\left[ -\frac{\left[ x - x_0 - \frac{a^2}{2b} \right]^2}{a^2} \right] dx ,$$

where we put $x_0 > 0$.

In the case $x_0 \gg a$,

$$g(x_0) = \frac{1}{a\sqrt{\pi}} \int_{-\infty}^{\infty} \exp\left[ -\frac{\left[ x - x_0 + \frac{a^2}{2b} \right]^2}{a^2} \right] dx = 1 ,$$

and

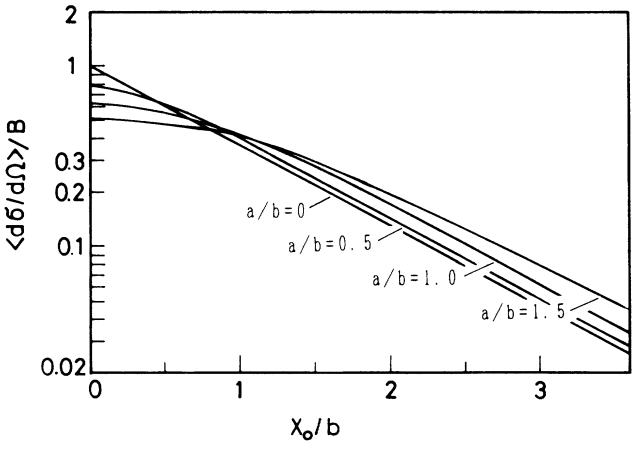


FIG. 10. Influence of the finite angular resolution of the apparatus upon measured DCS's. The horizontal axis expresses a reduced angle in unit of $1/b$, while the longitudinal axis expresses measured DCS. Here we take the true DCS as $d\sigma/d\Omega = B \exp(-|x|/b)$.

$$\left\langle \frac{d\sigma}{d\Omega} \right\rangle = B \exp(-x_0/b) \exp\left[ \frac{a^2}{4b^2} \right]$$

$$= \left[ \frac{d\sigma}{d\Omega} \right]_{x=x_0} \exp\left[ \frac{a^2}{4b^2} \right] .$$

We show in Fig. 10 how $\langle d\sigma/d\Omega \rangle$ is affected by the finite angular resolution, for the cases $a/b=0.5$, 1, and 1.5. Measured DCS $\langle d\sigma/d\Omega \rangle$ becomes much smaller than true DCS $d\sigma/d\Omega$ in the region where $x_0/b$ is smaller than $a/b$, but becomes slightly larger than $d\sigma/d\Omega$ in the region where $x_0/b$ is larger than $a/b$.

From Fig. 4, the full width at half maximum of the angular response function is 0.8°, so we get $a=0.48°$. From Fig. 7, we get $b=1.08°$ for the $(^2P_{1/2})4s$ excitation at $E=400$ eV, so $a/b=0.44$. The smallest scattering angle adopted in the present experiment is 1.8°, so $x_0/b = 1.8/1.1 = 1.64$.

From Fig. 10, we can see that we measured $d\sigma/d\Omega$ in the region where the measured values are larger than the true $d\sigma/d\Omega$ by the factor of $\exp(a^2/4b^2)=1.0$. For elastic scattering, $d\sigma/d\Omega$ decreases more slowly and $b$ is large, for instance, $b=7.0°$ at $E=400$ eV, so measured $\langle d\sigma/d\Omega \rangle$ is not significantly affected by the resolution $(a/b=0.07)$.

We determined $(d\sigma/d\Omega)_{\text{inel}}$ relative to $(d\sigma/d\Omega)_{\text{el}}$ using Eq. (2), so our measured values are systematically 5% larger, if the preceding argument strictly holds.


[1]G. P. Li, T. Tagayanagi, K. Wakiya, and H. Suzuki, Phys. Rev. A (to be published).

[2]J. P. de Jongh and J. van Eck, Physica (Utrecht) **51**, 104 (1971).

[3]J. W. McConkey and F. G Donaldson, Can. J. Phys. **51**, 914 (1973).

[4]J. E. Mentall and H. D. Morgan, Phys. Rev A **14**, 954 (1976).

[5]A. Chutjian and D. C. Cartwright, Phys. Rev. A **23**, 2178 (1981).

[6]K. Jost, J. Phys. E **12**, 1006 (1979).

[7]J. P. Bromberg, J. Chem. Phys. **61**, 963 (1974).

[8]R. H. J. Jansen, F. J. de Heer, H. J. Luyken, B. van Wingerden, and H. J. Blaauw, J. Phys. B **9**, 185 (1976).

[9]H. Bethe, Ann. Phys. **5**, 325 (1930).

[10]K. N. Klump and E. N. Lassettre, J. Chem. Phys. **68**, 886 (1978).

[11]G. E. Chamberlain, J. G. M. Heideman, J. A. Simpson, and C. E. Kuyatt, *Abstracts in Proceedings of the Fourth International Conference on the Physics of Electronic and Atomic Collisions, Quebec, 1965,* edited by L. Kerwin and W. Fite (Science Bookcrafters, Hastings-on-Hudson, 1968).

[12]G. M. Lawrence, Phys. Rev. **175**, 40 (1968).

[13]D. N. Stacey and J. M. Vaughan, Phys. Lett. **11**, 105 (1964).

[14]E. L. Lewis, Proc. Phys. Soc. **92**, 817 (1967).

[15]J. D. Dow and R. S. Knox, Phys. Rev. **152**, 50 (1966).